Research on the Influence of Contact Parameters on the Wear Characteristics of Fixture-bar Friction Pair in Low-stress Cropping

Weijian Guo
China University of Petroleum (East China)
Hang Wang
China University of Petroleum (East China)
Jishao Tao
China University of Petroleum (East China)
Ning Yang
China University of Petroleum (East China)
Bohan Yang
China University of Petroleum (East China)
Shulin Fu
China University of Petroleum (East China)
Jiayi Xu
China University of Petroleum (East China)
Tao Liu
China University of Petroleum (East China)
Linhan Gou
China University of Petroleum (East China)
Lijun Zhang (zlj-2@163.com)
China University of Petroleum (East China)

Research Article

Keywords: Low-stress cropping, Fixture-bar friction pair, Archard model, Radial wear degree, Acoustic emission

Posted Date: July 28th, 2021

DOI: https://doi.org/10.21203/rs.3.rs-744540/v1

Research on the influence of contact parameters on the wear characteristics of fixture-bar friction pair in low-stress cropping

Weijian Guo, Hang Wang, Jishao Tao, Ning Yang, Bohan Yang, Shulin Fu, Jiayi Xu, Tao Liu, Linhan Gou, Lijun Zhang*

College of Mechanical and Electronic Engineering, China University of Petroleum (East China), Qingdao 266580, China

Abstract: New structure of grooved fixture with cambered surface is proposed to reduce wear of bar surface caused by fixture in low-stress cropping. The influence of fixture contact parameters and surface quality on wear characteristics of fixture-bar friction pair is researched by using FEM and orthogonal experiment. The radial wear degree is proposed to evaluate the wear degree of bars under four contact conditions, and the wear mechanism of the friction pair is analyzed by SEM. AE-stress-strain cropping platform is established to research the influence of roughness on the comprehensive wear state of the friction pair. Results indicate that the friction pair under $A_4B_1C_2D_1E_4$ combination of contact parameters has the best wear reduction effect and lowest radial wear degree which is 0.0469mm^2 and 34.50% lower than one of line contact. AE characteristic parameters curves reflect that under different contact condition, when Ra=0.4μm, the values of AE characteristic parameters are all the minimum and comprehensive wear state of the friction pair is the best.

Keywords: Low-stress cropping; Fixture-bar friction pair; Archard model; Radial wear degree; Acoustic emission

0 Introduction

Precision cropping is widely used in aerospace, mechanical standard accessories, electronic components etc., which is the first process of metal forming [1-2]. Now the trend of cropping methods is green and efficient low-stress cropping [3-5]. However, under the existing low-stress rotating bending loading condition [6], the line contact form of fixture-bar friction pair causes the bar to produce slight shake relative to the fixture, and the reaction force of fixture will cause unstable extrusion deformation on the surface of bar. These issues not only cause uneven grinding marks on bar surface, but also cause collapse angle of the bar and poor surface quality [7-8]. At the same time, the impact vibration caused by friction and wear also affects working stability of cropping machine [9]. Therefore, it is very significant to research the influence of fixture contact parameters on the wear characteristics of friction pair under different contact conditions.

At present, domestic and foreign scholars have studied the wear mechanism of friction pairs under different materials and environments. Zhu et al. [10] carried out the rolling wear test of bainite wheel steel by using a double-disk rolling friction-abrasion testing machine. The results indicated that the contact stress would significantly affect the wear amount in the fatigue wear stage, and the range of contact stress would affect the grain refinement and process of growth in the material microstructure. Li et al. [11] studied the friction and wear properties of nickel matrix composites from room temperature to 600℃, and obtained that the friction coefficient of the composites increased first and then decreased with the increase of temperature. Taimin Gong et al. [12] established the wear mechanism diagram of copper-based friction clutch material under oil lubrication condition according to the measured wear rate, and divided it into super mild, mild and severe wear characteristics, and gave the linear equation of regional transition. Mukhacheva T.L et al. [13] applied Kragelsky yield criterion to study the friction and wear properties of medium carbon steel after carbonitriding in urea electrolyte. The consequence showed that the wear resistance of

* *Corresponding author. FAX: +86-532-86983500*
E-mail address: zlj-2@163.com (Lijun Zhang)

the steel increases by 40 % after carbonitriding at 750℃ for 7 min and sliding speed of 0.4~0.55m/s. Subba Rao Medabalimi et al. [14] used the pin-on-disk tribometer to evaluate the friction and wear behavior of partial oxidation of flame sprayed Ni-Fe-Si coating on the microstructure of the coating. The results specified that the wear rate of the coated steel is 5 times lower than that of the uncoated steel at 600℃, and the wear rate and friction coefficient of the coating decrease with the increase of temperature. Jinhua Lu et al. [15] studied the effect of pre-impregnated silicone layer on friction and wear properties of paper-based friction materials. The upshot expressed that the addition of a small amount of silicone into the paper-based friction material could improve the static friction coefficient of the paper-based friction material, but also reduce the dynamic friction coefficient and wear rate of the paper-based friction material. When the content of silicone was 7.5 %, the paper-based friction material had the highest static friction coefficient and the best stability. Slawomir Wos et al. [16] studied the effect of graphite surface texture on dry plane contact friction reduction performance of graphite-steel sliding pair and tested four different types of texture surface of graphite disk with the diameter of 100 mm and thickness of 10 mm. The results showed that the convergence direction of the bottom texture had a great influence on the dispersion of the friction coefficient. The disc texture with the bottom step parallel to the herringbone arm had a high stability and low friction coefficient, and the friction is small when the angle between the arms was 120°.

It can be found that the current research mainly focuses on the wear mechanism of friction pairs under different materials and environmental conditions, while the influence of contact parameters on the wear characteristics of friction pair is ignored. So this paper designs a new structure of fixture contact cambered surface based on the principle of tribology, and uses the method of combining orthogonal test and finite element simulation to study the influence of fixture contact parameters on the wear characteristics of friction pair and obtain the optimal combination of contact parameters. The evaluation index that affects the wear characteristics of the friction pair is proposed; On this basis, cropping test is carried out by combining with acoustic emission and stress-strain measurement technology to further determine the surface quality parameters of the bar under the optimal wear characteristics; and the SEM is used to analyze the micro-wear mechanism of the friction pair in order to comprehensively improve the surface quality of bar.

1 The principle of low-stress rotary bending cropping

The low-stress cropping machine is based on hydraulic compensation, which makes full use of stress concentration effect, hydraulic compensation technology and centrifugal effect to precisely crop metal bar and tube. It is mainly composed of six parts: frequency conversion motor, hydraulic transmission system, double slider mechanism, cropping die, mobile fixture mechanism and frame, as shown in Fig. 1(a). In the cropping process, one end of the bar with V-shaped groove is put into the cropping round hammer, and the other end is fixed with a fixture. Then the three-phase AC motor drives the hammer head to rotate at a high speed through the spindle. Due to the high speed of the hammer head, its smaller mass and radius of rotation produce a larger centrifugal force, which makes the slider slide eccentrically under the action of centrifugal force. At the same time, the hydraulic cylinder supplies oil to make the round slider slide in the radial groove, so as to compensate the centrifugal force. Under the combined action of centrifugal force and hydraulic compensation force, cracks at the tip of V-shaped groove initiate and propagate stably along the desired path, thus achieving low-stress brittle fracture [17]. In the process of cropping, the fixture and the bar are in contact and shake, which makes the bar wear greatly, and largely determines the surface quality of the bar. Among them, the mobile fixture mechanism of the low-stress cropping

machine is mainly composed of a movable fixture support, a guide pillar, a VH-305 hydraulic three-claw chuck, a bar, and a fixed fixture support, as shown in Fig. 1(b). The enlarged diagram of contact principle between the fixture and the bar is shown in Fig. 1(c), the yellow line is the bar, the overlapping part of the blue and yellow lines represent the contact zone between the fixture and the bar, and the pink arrow represents the extrusion deformation zone on the surface of the bar after being stressed. At the beginning of contact, the fixture and the bar are in line contact, under the combined action of hydraulic compensation force of hammer head and centrifugal force, while the bar near the fixture end shakes slightly, and the reaction force of fixture produces continuous extrusion on the bar surface, causing obvious wear and extrusion deformation. Moreover, under the condition of line contact, during the circumferential loading process, the shaking of the bar relative to the fixture will be more severe, making the extrusion wear of the bar surface more serious [18], as shown in Fig. 2. Therefore, it is of great significance to research the influence of contact parameters on the wear characteristics of friction pair under the different contact conditions.

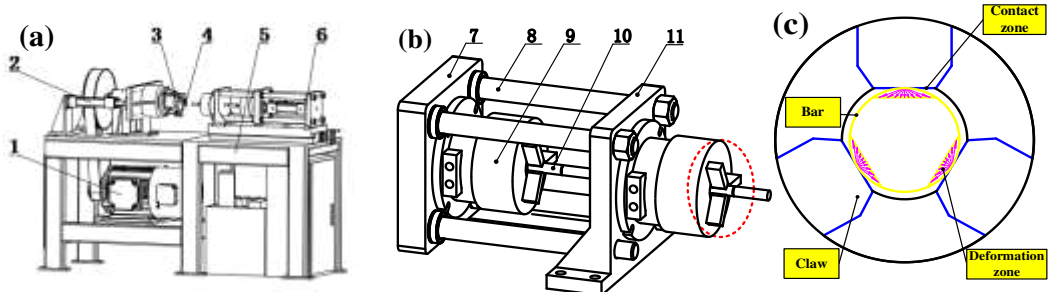

1-Variable frequency motor; 2-Hydraulic system; 3-double-slider mechanism; 4-Cropping die; 5-Mobile fixture mechanism; 6-frame; 7-Mobile fixture support; 8-Guide pillar; 9-VH305 Hydraulic three claw chuck; 10-Bar; 11-Fixture support

(a) Overall drawing of cropping machine (b) Schematic diagram of fixture assembly (c) enlarged diagram of contact principle between fixture and bar

Fig. 1 Contact principle diagram of fixture of low-stress cropping machine

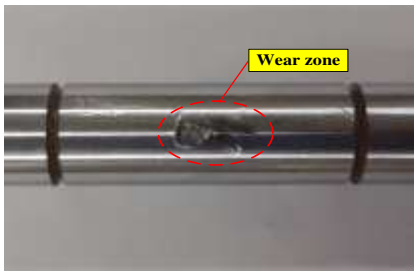

Fig. 2 Extrusion wear diagram of bar surface

2 Optimization of contact parameters of fixture in low-stress cropping

This section mainly analyzes the rationality of the cambered surface grooving structure of the fixture. On this basis, orthogonal experiment is designed to obtain the optimal combination of contact parameters in the fixture cambered surface grooving structure, so that the wear characteristics of friction pair are the best. Considering the complexity of the cambered fixture structure model, processing cost and cycle, the combination method of finite element simulation and orthogonal experiment is adopted to analyze in this section.

2.1 Wear simulation analysis based on Archard model

2.1.1 Establishment of finite element analysis model of friction pair

Because the contact parameters between fixture-bar will affect the surface quality of bar, a new

type of contact cambered structure of hydraulic clamping claw is designed according to the tribology theory. The clamping claw is made of wear-resistant materials, and the main V-grooves and the auxiliary friction increasing grooves of equal width are set on the cambered surface, and the rounded corners are arranged on the V-groove edge to reduce the contact wear of the fixture-bar friction pair. The combined fixture-bar model is divided into three contact zones according to the working state: the hydraulic compensation force F_h of the hammer head on the bar is taken as the benchmark; the clamping claws are marked as 1~3 clockwise respectively; the corresponding contact zones between the clamping claws and the bar are I~III respectively. The finite element model of fixture-bar friction pair is shown in Fig. 3(a), and the contact parameters are shown in Fig. 3(b). Among them, the linear contact model and the cambered grooving contact model only have different contact conditions, which can be done by referring to Fig. 1(c).

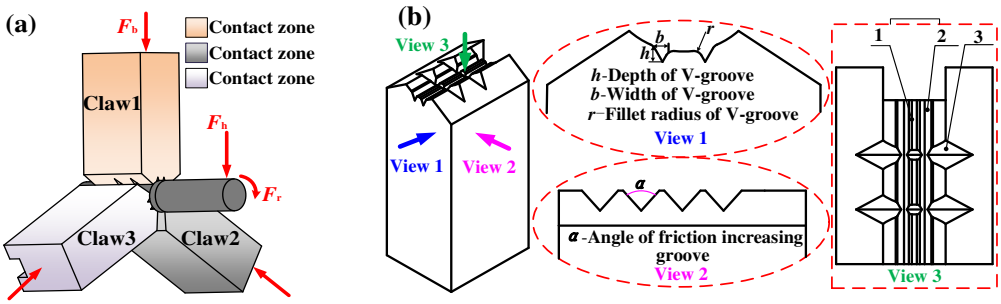

1- Fillet radius of V-groove; 2- V-groove; 3- Auxiliary friction increasing groove

(a) Mechanical model of fixture-bar (b) Schematic diagram of fixture bar contact parameters

Fig. 3 Three dimensional model of fixture-bar friction pair

2.1.2 Define material propertiesss

Using Archard wear simulation analysis method, the fixture material is low carburizing steel of 20CrMnTi; the bar material is 45# steel; the hammer head material is GCr15. The performance parameters of the material are shown in Table 1.

Table 1 Performance parameters of material

Material	Mechanical parameters			
	ρ/g/cm^3	E/GPa	ν	$\sigma_{s/MPa}$
45#	7.89	210	0.269	355
GCr15	7.83	209	0.30	518.42
20CrMnTi	7.80	207	0.25	835

2.1.3 Division of self-adaptive mesh

Because of the complex structure of fixture's contact surface and the existence of irregular small surface, it can only be divided into tetrahedral grid by automatic division method, and the grid quality can be controlled by improving the cell size. Using Multizone method, bar and bearing are set as hexahedral grid and Face Meshing is used to ensure the uniformity of end face mesh shape. The mesh unit size is controlled to be 0.15mm. After solving, the model is symmetrically divided into 82167 units, 118,637 nodes, and the grid quality is high with the highest of 0.99972 and average is 0.84472. The effect of the multizone meshing model is shown in Fig. 4.

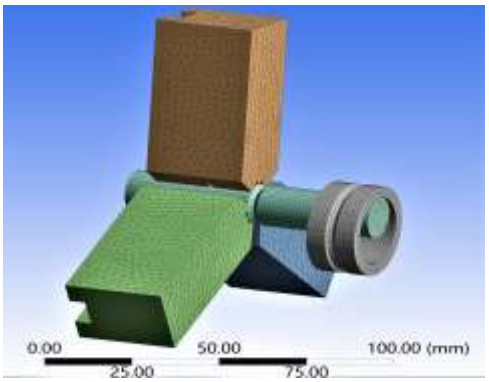

Fig. 4 Mesh generation model of friction pair

2.1.4 Define boundary conditions

One end of the bar is clamped by the hydraulic clamping claws; the clamping force F_b=10kN; the bearing hammer head acts on the other end of the bar; the rotational speed is 600rpm. Under the joint action of the centrifugal force F_r generated by the spindle driving the rotation of the hammer head and the hydraulic compensation force F_h generated by the feeding cylinder pushing the hammer head sliding, the rotary bending loading of the hammer head on the bar is realized. At the same time, motion joints are established to apply the corresponding load and speed, and the end face of the bar could move axially. Archard wear model [19] is used, and its form is shown in Eq. (1):

$$\dot{W} = \frac{K}{H} P^m v_{rel}^{\ n} \tag{1}$$

Where: $\dot{W}$ is the wear volume (mm^3); K is coefficient of wear; H is material hardness (MPa); P is normal contact pressure (MPa); v_{rel} is relative motion velocity of friction pair (m/s); m is contact pressure index; n is relative velocity index. Among them, the wear coefficient K is determined by referring to literature [20]. Hardness is 1/3 of the yield strength of the material σ_s. By calling the command flow of APDL wear model, the hardness, wear coefficient, speed and pressure index of materials are input to realize the wear simulation calculation of fixture-bar friction pair.

2.1.5 Comparative analysis of simulation results

The transient dynamic analysis of the friction pair is carried out, and the correlation results of the friction pair under the linear contact and cambered surface contact for 10s are obtained as follows.

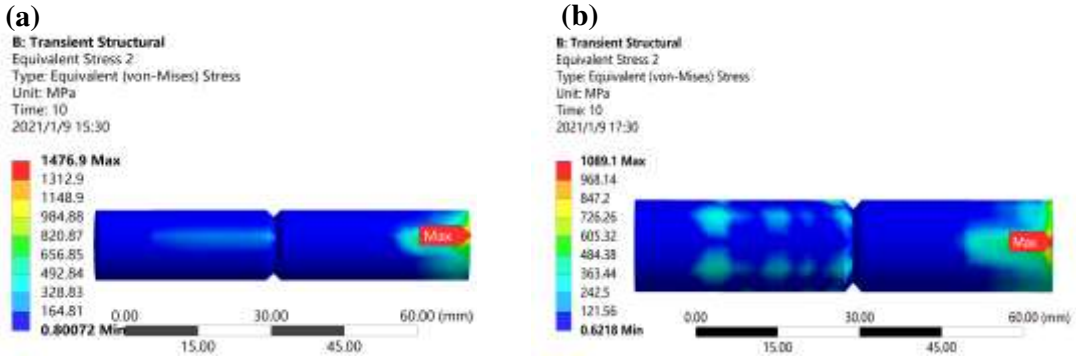

(a) Equivalent stress nephogram of line contact bar (b) Equivalent stress nephogram of cambered contact bar

Fig. 5 Equivalent stress nephogram of bar under different contact conditions

Fig. 5(a) and (b) are the equivalent stress nephogram of the bar in linear contact and cambered contact respectively. Fig. 5 shows that under the same working condition, different contact conditions of fixture make the deformation of the extrusion surface at the clamping end of the bar

different, thus affecting the stress state of the bar. Under the linear contact condition, the bar has slight torsional deformation due to the centrifugal force acting on the bar, and then an approximate linear stress change zone slightly wider than the contact surface of the claw appears at the bar clamping end, and the stress zone is relatively uniform. The maximum equivalent stress of the bar appears at the contact point between the bearing and the bar, and its value is 1476.9MPa. Under the cambered surface contact condition, the maximum equivalent stress of the bar appears in the same position as that of the linear contact. However, since the normal contact load applied is the same, and the contact zone is larger and the stress value is lower than that of the linear contact, which is 1089.1MPa.

According to the nephogram of axial sliding distance of the bar in Fig. 6, under both linear contact and cambered contact, the maximum occurs in the contact zone between the fixture and the bar. The difference is that the maximum axial sliding distance of the bar clamping end is 18.70μm in linear contact. In cambered contact, because of the existence of auxiliary friction increasing grooves on fixture contact surface, the axial sliding of bar is effectively reduced. Therefore, the maximum axial sliding distance of the clamping end is 8.11μm, which is significantly lower than that of the linear contact condition.

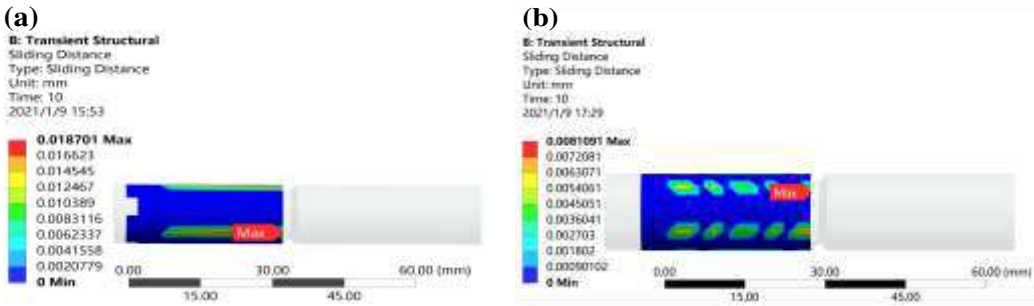

(a) Nephogram of axial sliding distance of line contact bar (b) Nephogram of axial sliding distance of cambered contact bar

Fig. 6 Nephogram of bar axial sliding distance under different contact conditions

By comparing the wear volume curves Fig.7(a) of the two contact conditions, it is indicated that the change trend of the wear volume curves of the bars is roughly the same. The volumetric wear rate of the three contact zones of the fixture-bar friction pair increases rapidly in 0~3s, then decreases gradually in 3~6s, and remains basically unchanged with the increase of time after 6s. According to the typical wear process curve [21], under the condition of constant working conditions, 0~6s is the period when the running stage of the friction pair approximately ends, and 6~10s is the stable wear stage when the friction pair is working normally. Therefore, the result of the wear curve is reasonable. According to the comparative analysis, in linear contact, the maximum wear volume in the contact zone 3 of the friction pair at 10s is 0.61904mm^3; the minimum wear volume in contact zone 1 is 0.40502mm^3. In cambered surface contact, the maximum wear volume in contact zone 2 of the friction pair is 0.55829mm^3 at 10s; the minimum wear volume in contact zone 1 is 0.49480mm^3. By comparing the friction stress curve Fig.7(b), it is found that the friction stress of the friction pair changes uniformly in the case of linear contact. Under the combined action of centrifugal force and normal contact pressure that the bar will undergo slight torsion and extrusion deformation makes the contact zone of friction stress increase. Under the same contact pressure, the friction stress will decrease, which will cause the bar to sliding slightly in the radial and axial direction, thus increasing the wear of the bar surface. Among them, the maximum average friction

stress in contact zone 2 at 10s is 36.2211MPa; the minimum average friction stress in contact zone 3 is 13.1469MPa. In cambered surface contact, due to the effect of the main V-groove and the auxiliary friction-increasing groove on the bar surface, the friction stress of the bar increases as a whole compared with that of the linear contact, and the circumferential torsion and axial sliding of the bar are improved. Among them, the maximum average friction stress in contact zone 1 is 51.6070MPa; the minimum average friction stress in contact zone 2 is 15.1038MPa.

By comparing the simulation results, it can be seen that the wear volume of the bar in cambered surface grooving contact is lower than that in linear contact, and the torsion and axial sliding effect of the bar are significantly reduced, which improves the surface quality of the bar. Therefore, it is reasonable to design the fixture's contact surface and optimize the contact parameters to improve the wear characteristics of the friction pair.

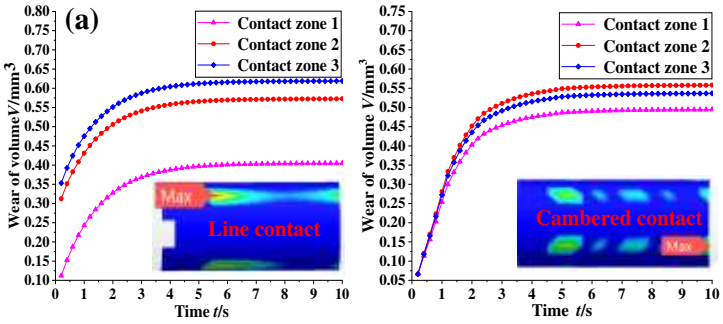

(a) Wear law of bar under different contact conditions

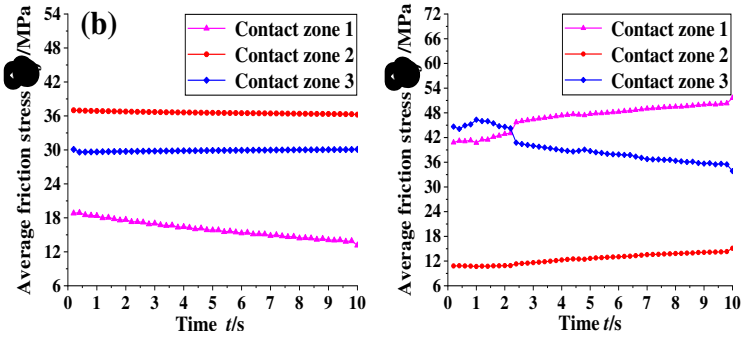

(b) Friction stress law of bar under different contact conditions

Fig. 7 Friction and wear law of bar surface under different contact conditions

2.2 Determination of Optimal Combination of Contact Parameters of Cambered Surface Fixture

As shown in Fig. 3 (b), there are many contact parameters of the cambered surface fixture. According to the simulation results of 2.1.5: under the same rotational speed and load condition, although the wear reduction effect of cambered grooved contact is better than that of line contact, the influence of fixture contact parameter combination on the wear characteristics of friction pair is not considered. Therefore, the orthogonal experiment is designed to further optimize the contact parameters of 2.1.1 cambered surface grooving fixture model, so as to obtain the optimal combination of contact parameters of cambered surface grooving fixture.

2.2.1 Orthogonal experimental design scheme

Because the wear characteristics of the friction pair of cambered grooved fixture and bar are affected by many contact parameters; the orthogonal experiment is designed in order to reduce the wear degree of friction pair. According to the structural characteristics of fixture contact surface, five factors such as the opening angle of auxiliary friction increasing grooves α, the number of

fixture auxiliary friction increasing grooves, V-shaped groove edge fillet radius *r*, V-shaped groove depth *h* and width *b* are selected; four levels of each factor are selected. The factor level table is shown in Table 2. Design $L_{16}(4^5)$ orthogonal test table, as shown in Table 3. Only 16 orthogonal tests are needed to reflect 4^5=1024 comprehensive tests [22].

Table 2 Contact parameter factor level table

Levels	Factors				
	Groove depth *h*/mm	Groove width *b*/mm	Fillet radius *r*/mm	Angle *α*/°	Number of friction increasing grooves
1	1.5	1.4	0.2	45	3
2	2.0	1.7	0.3	60	6
3	2.5	2.0	0.4	75	9
4	3.0	2.3	0.5	30	12

Table 3 Orthogonal test table of contact parameters

Orthogonal group	Groove depth *h*/mm	Groove width *b*/mm	Fillet radius *r*/mm	Angle *α*/°	Number of friction increasing grooves
1	1.5	1.4	0.2	45	3
2	2.0	1.7	0.3	45	6
3	2.5	2.0	0.4	45	9
4	3.0	2.3	0.5	45	12
5	2.0	2.0	0.2	60	12
6	1.5	2.3	0.3	60	9
7	3.0	1.4	0.4	60	6
8	2.5	1.7	0.5	60	3
9	2.5	2.3	0.2	75	6
10	3.0	2.0	0.3	75	3
11	1.5	1.7	0.4	75	12
12	2.0	1.4	0.5	75	9
13	3.0	1.7	0.2	30	9
14	2.5	1.4	0.3	30	12
15	2.0	2.3	0.4	30	3
16	1.5	2.0	0.5	30	6

2.2.2 Analysis results of orthogonal optimization of fixture contact parameters

The transient dynamic simulation of 16 groups of orthogonal models under the cambered surface grooved contact is carried out, and the relevant wear results of friction pairs are obtained as shown in Table 4.

Table 4 Wear simulation results of fixture-bar friction pair

Orthogonal group	Average friction stress $\bar{\sigma}_f$/MPa	Average axial sliding distance $\bar{s}$/μm	Wear of volume *V*/mm^3
1	178.4453	64.21	1.6576
2	140.0467	59.38	1.7001
3	54.5320	25.74	1.5524
4	33.8203	7.95	1.5904
5	229.6633	56.92	1.5743
6	88.9403	66.72	1.4155
7	157.2530	34.88	1.1750
8	144.3467	66.23	1.9275
9	183.1433	67.82	1.9756
10	274.0067	55.59	1.7990
11	232.6600	38.64	2.3156
12	57.1790	17.51	1.1368
13	173.92	31.12	1.6144
14	23.5407	9.98	1.3507
15	100.9383	76.78	1.8762
16	148.98	66.74	2.0272

Table 5 shows the optimization results of contact parameters of friction pair under cambered

contact. In order to show the friction and wear characteristics of bar more intuitively, the average axial sliding distance and wear volume of bar surface at 10s are selected as the evaluation indexes of orthogonal test. The optimal level and the primary and secondary factors are obtained by using the comprehensive balance range analysis method [23], and then the optimal combination of fixture contact parameters in the design table is obtained. In Table 5, A, B, C, D and E represent groove depth, groove width, groove edge fillet radius, friction increasing grooves angle and the number of friction increasing grooves respectively, and k1, k2, k3, k4 respectively represent the average value of the test data when the factor is taken at the corresponding level. R is the range value of each factor to the test index. The influence degree of each factor on the test index is determined by the range value.

Table 5 Optimization result of fixture cambered contact parameter

Cambered contact f=0.2						
Evaluation index	Average	A	B	C	D	E
Average axial sliding distance $\bar{s}$/MPa	k1	59.078	31.645	55.018	39.320	65.703
	k2	52.648	48.843	47.918	56.188	57.201
	k3	42.443	51.248	44.010	44.890	35.273
	k4	32.385	54.818	39.608	46.155	28.373
	R	26.693	23.173	15.410	16.868	37.330
	Better level	A_4	B_1	C_4	D_1	E_4
	Impact of factor	2	3	5	4	1
Wear of volume V/mm^3	k1	1.8540	1.3300	1.7055	1.6251	1.8151
	k2	1.5719	1.8894	1.5663	1.5231	1.7195
	k3	1.7016	1.7382	1.7298	1.8068	1.4298
	k4	1.5447	1.7144	1.6705	1.7171	1.7071
	R	0.3093	0.5594	0.1635	0.2837	0.3853
	Better level	A_4	B_1	C_2	D_2	E_3
	Impact of factor	3	1	5	4	2

It can be seen from Table 5 that the most important factor affecting the axial sliding distance of the bar surface is the number of auxiliary friction increasing grooves, and the range value R=37.33. The second influencing factors are the groove depth and width. According to Table 2 and 3, the increase in the number of auxiliary friction grooves can effectively reduce the axial sliding of the bar surface and the wear loss of the friction pair. The groove width is the most important factor affecting the wear extent of bar, and the range value is R=0.5594. The second influencing factors are groove depth and the number of auxiliary friction grooves. Because the contact deformation is considered in the simulation model, the wider the V-shaped groove is, the smaller of contact zone between the two friction pairs is. Under the same normal load, the friction stress of the contact surface magnifies and the wear extent increases [24-25]. And the auxiliary friction increasing grooves can increase the fastening state of the friction pair, reduce the surface wear caused by the axial movement of the bar surface, and play a role in reducing wear.

Regarding the results of the axial sliding distance of the bar surface, the combination of the better level column is $A_4B_1C_4D_1E_4$; As for the results of wear volume, the combination of the column of better level is $A_4B_1C_2D_2E_3$. Therefore, A_4 is the best groove width and B_1 is the best groove depth. Combined with the analysis of the range value, the influence of the groove edge fillet radius (C) on the axial sliding distance and the wear volume ranks fifth, and there is an influence value C_3 between the axial sliding distance C_2 and C_4, and the wear volume C_2 is the best, followed by C_4. Considering

the two indexes comprehensively, the groove edge fillet half diameter C_2 is appropriate; the influence of friction increasing groove angle D on the axial sliding distance and wear volume is the fourth, and the gap between the axial sliding distance D_1 and D_2 is large, while the gap between the wear volume D_1 and D_2 is small. Considering the two indexes comprehensively, the effect of friction groove angle D_1 is better. The influence of the number of auxiliary friction grooves E on the axial sliding distance is the first, and the influence on the wear volume is the second, and E_3 is better than E_4 in terms of wear volume. Comprehensive consideration, E_4 level is better for auxiliary friction increasing groove. The optimal combination of fixture contact parameters under cambered surface grooved contact is $A_4B_1C_2D_1E_4$. That is, when the groove depth h is 3.0 mm; the groove width b is 1.4 mm; the groove edge fillet radius r is 0.3 mm; the auxiliary friction increasing groove angle α is 45 °, and the number of auxiliary friction increasing grooves are 12, and the friction pair has the best wear characteristics.

3 Experimental verification of wear characteristics of friction pair contact parameters

3.1 Establishment of radial wear degree model

The optimal combination of cambered contact parameters of fixture is obtained through 2.2.2 orthogonal experiment, which needs comparative analysis. According to Table 4, the boundary values of axial sliding distance and wear volume are in different orthogonal groups. Therefore, it is necessary to establish comprehensive evaluation indexes of axial sliding distance and wear volume, so that the test data can better reflect the wear characteristics of bar surface. The initial contact length of the fixture-bar is set as S_0, since the friction pair is continuous contact, and the initial contact section of the fixture-bar is regarded as a wear element. After the time interval $\triangle t_i$, the average sliding distance of wear element is $\triangle \overline{S}_i$. After 10s, the average axial sliding distance of the bar is $\overline{S} = \sum \Delta \overline{S}_i$. The ratio of the wear volume V to the average axial sliding distance $(S_0 + \overline{S})$ of bar is defined as the radial wear degree λ of bar. The boundary value of λ is obtained through analysis as the comparative analysis group of fixture, and the model of radial wear degree is shown in Fig. 8.

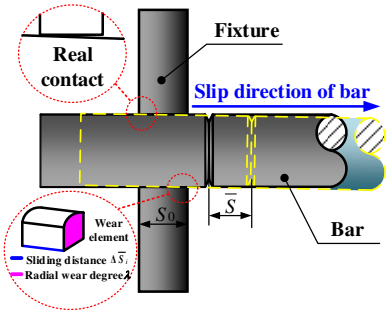

Fig.8. Model of radial wear degree of bar

The simulation results of wear volume and axial sliding distance of 16 groups of models are substituted into the radial wear degree model of bar, and the radial wear degree of bar is obtained as shown in Table 6. From Table 6, the radial wear degree λ of orthogonal group 11 is the largest and that of orthogonal group 12 is the smallest at 10s. According to the wear characteristics of fixture-bar friction pair, friction and wear tests are carried out on claws with four different contact conditions: optimal combination of cambered contact parameters, line contact, orthogonal groups 11 and 12.

Table 6 Simulation results of radial wear degree of 16 groups of bar

Orthogonal group	Radial wear degree λ/mm^2	Orthogonal group	Radial wear degree λ/mm^2
1	0.0661	9	0.0788
2	0.0678	10	0.0718
3	0.0620	11	0.0925
4	0.0636	12	0.0454
5	0.0628	13	0.0645
6	0.0565	14	0.0540
7	0.0469	15	0.0748
8	0.0769	16	0.0809

3.2 Experimental steps and platform construction

KM-001 Rotary bending low-stress cropping machine [26], DS2 series full information acoustic emission signal analysis system and stress-strain gauge were used to verify the cropping experiment. And, the cropping principle is shown in Fig. 9 and the construction of experimental platform is shown in Fig. 10. The strain gage was connected to the stress-strain gauge and affixed near the contact zone of bar and bearing, half-bridge compensation was selected as the compensation method and strain measurement was used as the measurement method. The hydraulic compensating force F_h was acted as the concentrated force on the contact center between bar and bearing, the distance between the action point of force and the center of strain gage was L_1, and the distance between fixture near the end of V-shaped groove and strain gage was L_2. Under the rotary bending load of the bearing, the bar would produce a certain deflection, and the bar was equivalent to a cylindrical section. According to theory of mechanics of materials, the bending moment M satisfied the following Eq. (2) [27]:

$$W_z \varepsilon E = M = F_h (L_1 + L_2) \tag{2}$$

Where, W_z- modulus of bending section (mm^4); F_h-hydraulic compensation force(N); ε-value of bar strain measurement; E-elastic modulus (GPa). The strain of bar was measured by DHDAS dynamic signal acquisition and analysis system, and the hydraulic compensation force F_h of bearing to bar was calculated in the Eq. (2). For the clamping force F_b of the fixture, the bearing kept away from the bar, the fixed fixture retained only No. 1 claw, and the end of the bar was clamped by a moving fixture. The strain gage was affixed near the contact surface between fixed fixture and bar, and the bar was pressed by No. 1 claw driven by hydraulic cylinder. It was equivalent to the mechanical model of bearing press bar, the strain value was measured by stress-strain gauge, and then the clamping force F_b of claw was obtained. Therefore，load conditions were determined during the cropping process.

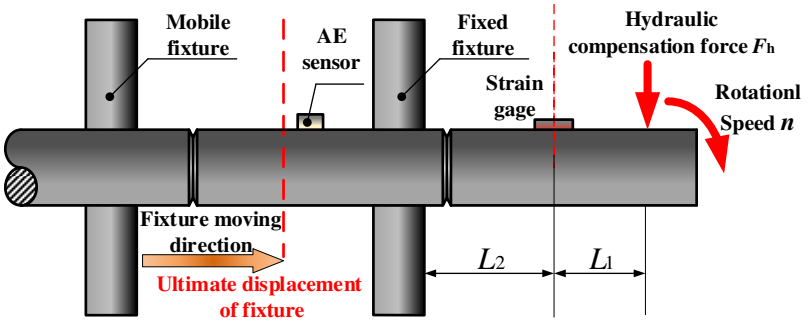

Fig. 9. Principle diagram of cropping experiment for friction pair

The hydraulic compensation force of bearing was F_h=1560N and the clamping force of single claw of clamp was F_b=10kN in the cropping experiment by the above method, the contact method of friction pair was cambered contact; the fixture-bar friction pair was fixed; the bearing rotates eccentrically along the bar axis; the radius of rotation R=8mm; the rational speed is 600rpm, and the motion time was 10s. The acoustic emission sensor was fixed near the contact zone between the fixture and bar by coupling agent, and the fixture-bar friction pair was worn by rotary bending loading. The continuous acoustic emission signal generated by wear was transmitted to the signal analysis system through the preamplifier, and the signal sampling frequency was 2.5MHz. Before the experiment, the initial contact position between the fixture and bar was marked. After the experiment, the axial sliding distance of the bar was measured, and then the bar was ultrasonically washed by acetone, then the wear amount of the bar was weighed on the inductive electronic balance of FA1004 with the accuracy of 10^{-4}g, and the microstructure of the wear mark on the bar surface was observed by SEM.

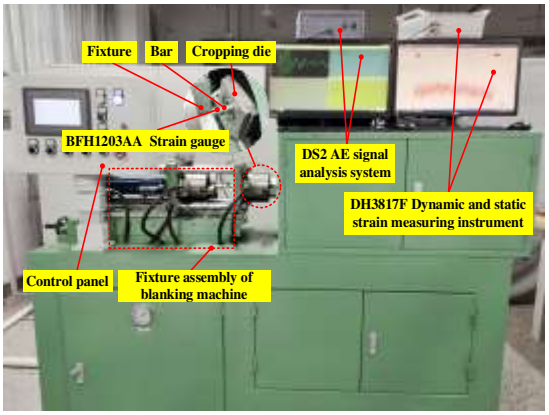

Fig. 10. Construction of cropping experiment platform for friction pai

3.3 Analysis of wear characteristics of friction pairs

3.3.1 Comparative analysis of radial wear degree

The overall mass of the bar was different due to the process flow, machining accuracy, internal structure or a little impurity. In order to ensure the accuracy of the test, the bar mass corresponding to the number should be weighed before the test of different fixture-bar wear friction pairs, and the mass loss associated with processing should be considered. The average value of each sample should be weighed five times. Finally, the bar mass parameters of the fixture contact part under four groups of different contact conditions were obtained. As shown in Table 7, where $\bar{m}_1$ was the original mass of the bar, $\bar{m}_2$ was the mass of the bar after cropping, $\triangle m_w$ was the mass loss of the bar wear, $\triangle m_c$ was the mass loss considering the processing.

Table 7 The mass result of bar material contact with fixture

Contact condition	Mass of bar in contact part of fixture			
	$\bar{m}_1$/g	$\bar{m}_2$/g	$\triangle m_w$/g	$\triangle m_c$/g
Optimal combination	54.4406	54.4312	0.0092	0.0002
Orthogonal.11th	54.5123	54.4956	0.0162	0.0005
Orthogonal.12th	54.6862	54.6751	0.0107	0.0004
Line contact	54.5412	54.5266	0.0143	0.0003

The relative axial sliding distance of fixture-bar friction pair during cropping test was measured. The actual value of the axial sliding distance of the bar was larger than the simulation value due to the factors such as the medium spindle pair of the cropping machine and the rigid vibration of the cropping machine. According to the initial distance S_0 of the bar and fixture and the wear mass $\triangle m_w$ of the bar, the average axial sliding distance of the bar was measured and the average value was

calculated by using the vernier caliper with the accuracy of 0.02 mm. The radial wear degree of the bar after the cropping test was calculated, as shown in Table 8.

Table 8 Radial wear degree of bar under four contact tests

Contact condition	Related parameters (S_0=25mm ρ=7.89g/cm^3)		
	$\overline{S}$ /μm	$\triangle m_w$/g	λ /mm^2
Optimal combination	120	0.0093	0.0469
Orthogonal.11th	220	0.0206	0.1034
Orthogonal.12th	180	0.0107	0.0538
Line contact	300	0.0143	0.0716

Fig. 11 shows the histograms of radial wear degree of bars obtained by simulation and experiment under four contact conditions. Overall, the experimental values of radial wear degree of bar under four contact conditions are greater than the simulation value, and the error value is about 6.71%~15.61% and the error is in the appropriate range. The reasons for the comprehensive analysis of the error are as follows: firstly, the average axial sliding distance of the bar increases due to the manufacturing accuracy of the cropping machine itself and the stiffness of the machine in the experiment; secondly, the bar is loaded by the hammer head in the cropping, resulting in a certain deflection, which changes the contact zone with the fixture and increases the wear amount; finally, because the friction coefficient of the fixture-bar friction pair is always changing in the experiment process, the bar wear obtained by the experiment will be larger than the simulation value.

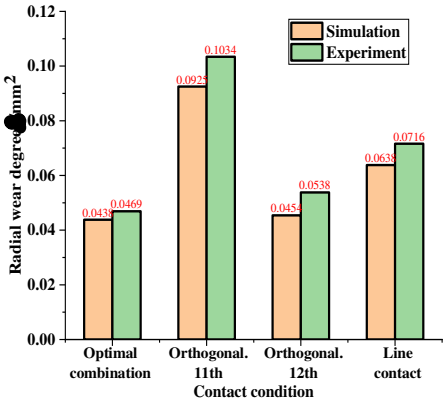

Fig. 11 Histogram of radial wear degree of simulation and experiment under different contact conditions.

In part, the number of auxiliary friction-increasing grooves, opening angle, groove depth and groove width of the main V-shaped groove are different under different contact conditions, so the radial wear degree fluctuates greatly. Under the same load and rotational speed, the minimum radial wear degree of bar under the optimal combination of contact parameters is 0.0469mm^2; the maximum radial wear degree of bar is 0.1034mm^2 under No.11 contact condition. Compared with the normal line contact condition, the radial wear degree of the bar is reduced by 34.50% under the optimal combination of contact parameters. The radial wear degree of bar under the orthogonal group 11 is increased by 44.41% compared with the ordinary line contact.

3.3.2 Wear mechanism analysis

Fig. 12 shows the wear surface morphology of 45# bar observed by scanning electron microscope at different magnifications under four contact conditions. It can be seen from Fig. 12(a) that there were some narrow and shallow scratches and plowings on the surface of the bar under this state. After the fixture contacts with the bar, due to the sliding of the bar relative to the fixture, the rough peak of the fixture was embedded in the bar surface to push and form plowings, and at the same time, abrasive particles were generated, so that the bar surface was abraded, and many narrow and shallow scratches were generated. At this time, the oxide layer on the bar surface was not

destroyed, and the main occurrence was abrasive wear. Fig. 12(b) shows the morphology of the orthogonal group No.12 amplified by 200 times. At this time, the surface of the bar was extruded and worn by the fixture. The slight plastic deformation on the surface made some adhesive nodes break and fall off to form wear debris, and adhesive wear occurred. Under the combined action of debris and abrasive particles, many wide scratches and pits with different depths appeared on the surface. With the relative movement of the friction pair, fine abrasive particles and wear debris formed a thin layer of mixture adhered to the worn surface during repeated extrusion, which reduced the wear of the bar surface to some extent. Fig. 12(c) shows the wear surface morphology of the orthogonal group No.11 amplified by 100 times. At this time, the extrusion of the fixture on the surface of the bar was more serious, and the oxide layer on the surface of the bar was destroyed, resulting in oxidative wear. The material was partially stacked on both sides, and the wear was more serious. At the same time, due to the poor brittleness of 45#, under the action of abrasive extrusion, a slight extrusion spalling phenomenon occurred on the surface, and the combined action of abrasive particles and debris generated wide scratches. Moreover, due to the relative motion of the friction pair, the random migration of abrasive particles and debris generated adhesive layers with different sizes. Fig. 12(d) shows the surface morphology enlarged by 150 times by linear contact. It can be seen that the extrusion of the fixture on the bar is more serious under this contact. Serious plastic deformation occurred on the surface of the bar, and the material transferred and accumulated to form a new adhesive layer. The oxide layers on the surface of the bar were destroyed to form oxide and solid solution crystallization [28-29], and new oxide layers were formed during the movement, which hindered the further wear of the bar to some extent.

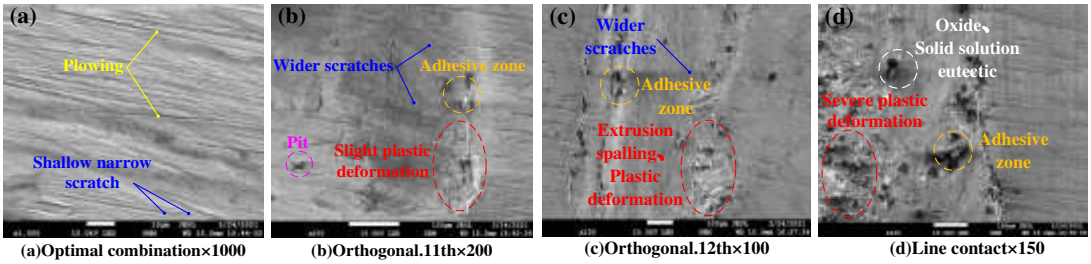

Fig. 12 Wear surface morphology of bar under different contact conditions

4 Determination of optimal surface quality based on acoustic emission

By observing the SEM morphology of bars in Fig. 12, it is found that there are many micro-convex peaks and concave valleys on the surface of bars under four contact conditions. According to relevant literature [30], these surface quality parameters have a great influence on the comprehensive wear characteristics of friction pairs under dry friction conditions. This section will focus on the influence of surface quality parameters on the comprehensive wear characteristics of fixture - bar friction pair.

4.1 Analysis of surface quality of fixture-bar friction pair

After the molding process, the contour of the fixture contact surface fluctuated, and its surface quality can be described by the roughness of the contour of the contact surface [31]. The model is shown in Fig. 13. Assume that the peak height of the processed fixture contact surface contour is P, the distance between any point in the peak contour zone and the ideal surface is y_i, and the distance between two adjacent peaks is D. According to the range of D, the surface quality is defined as roughness, corrugation and macro deviation. When D<1mm, the average arithmetic deviation of the absolute value of the distance from each point on the surface peak contour zone to the ideal

surface of the friction pair is defined as the surface roughness H_R, as shown in Eq. (3).

$$H_R = \frac{1}{L}\int_0^L |y_i| dx \tag{3}$$

According to the relevant data, the surface roughness of the friction pair has no obvious periodicity, and its peak height P is about 2~800μm, and the distance between adjacent peaks D is about 0.03~400μm. Various experiments show that due to the molecular interaction between the contact surfaces of the friction pair, sufficient roughness is needed to meet the requirements of wear resistance. Moreover, under different working conditions, smaller the roughness of the friction surface causing better wear characteristic does not always hold true. There is an optimal value HR0 for the surface roughness of the friction pair, when the wear characteristics of the friction pair reaches the optimum and the wear amount is the minimum [32].

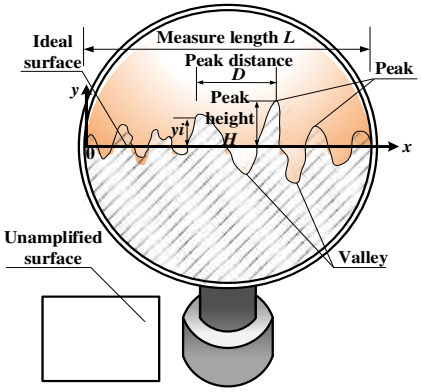

Fig. 13 Quality parameters of machined fixture surface

4.2 Establishment of acoustic emission model for elastic deformation of micro-convex body

The existence of micro-convex body on the surface of friction pair is the direct cause of surface roughness difference. In the relative motion, the elastic deformation occurred in the collision between the micro-convex bodies, and the continuous signal was released to reflect the wear characteristics of the friction pair. Therefore, in order to study the friction and wear characteristics of friction pair, continuous signal parameters related to the elastic deformation of the micro-convex body on the contact surface must be constructed to characterize the wear characteristics of friction pair. Combined with Hertzian contact theory and Greenwood-Williamson contact model, Yibo Fan et al. [33] established the relationship between elastic deformation of micro-convex bodies between contact surfaces of friction pairs and acoustic emission signals in the sliding process, and obtained the acoustic emission characteristic signal parameter RMS [34] that characterized the wear characteristics of friction pairs. As shown in Eq. (4).

$$V_{\text{rms}} = \frac{\sqrt{\frac{2}{5}K_e K_s N w v \int_y^\infty (z-y) f(z) dz}}{R_1^{\frac{1}{4}} \sqrt{\int_y^\infty \sqrt{z-y} f(z) dz}} \tag{4}$$

Where, $f(z)$ is Gaussian probability density function of the contour height of the contact surface; y is distance from convex surface to ideal plane (mm); K_e is the ratio of elastic energy of contact peak converted to AE signal; K_S is conversion rate of acoustic emission measurement system sensor to acoustic emission signal; N is total number of contact peak points between the contact zones of two friction pairs; w is load borne by peak point (N); v is surface sliding speed of friction pair (mm/s).

According to Eq. (4), for the conventional sliding friction process, when normal load and rotational speed are fixed, the acoustic emission characteristic parameter V_{rms} formed by the elastic deformation of the micro-convex body between friction pairs is mainly affected by the contact characteristic parameters on the surface of the friction pairs. Therefore, continuous acoustic emission characteristic signal parameter V_{rms} can be used to characterize the friction and wear characteristics of the material well, and the surface quality of the fixture under the optimal wear characteristics can be determined to guide the cropping experiments.

4.3 Experiment procedure

According to the roughness requirements of the fixture after surface processing and the GB/T1031-2009 surface roughness parameter table, it is determined that the range of fixture surface roughness Ra is 0.2μm~0.8μm. So the following roughness value was selected according to the standard value and supplementary value specified in GB: 0.2, 0.25, 0.32, 0.4, 0.5, 0.63, 0.8 (μm). #320, #400 and #600 sandpaper are used to polish the contact surface of the fixture first; #800 sandpaper to correct the flatness of the surface; 100% pure cotton dipped in alcohol and other cleaning solution to wipe the surface carefully, and finally the surface is polished. The surface roughness of polished sample was measured by TIME3202 hand-held surface roughness tester with accuracy of 0.001μm. In order to ensure the uniformity of the measurement results, each sample surface was measured 6 times to take the average value, and the measured value relative to the standard value allowed a certain floating accuracy. The experimental platform is shown in Fig. 14.

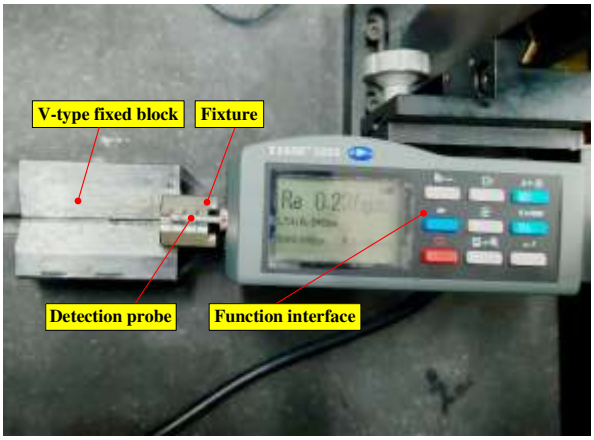

Fig. 14 Construction of fixture surface roughness test platform

4.4 Determination of optimal surface quality of fixture

Under four different contact conditions, the acoustic emission signal data of the fixture-bar friction pair are collected and analyzed, and the acoustic emission characteristic parameter curve characterizing the wear characteristics of the friction pair is obtained, as shown in Fig. 15. It can be found that under different contact conditions the differences of AE characteristic parameters such as amplitude, energy, RMS and ASL are obvious; the AE characteristic parameters reach the maximum value under orthogonal group 11 condition. While under the optimal combination of contact parameters, the value of AE characteristic parameters reaches the minimum. It can be seen from Fig. 11 that the radial wear degree of the bar under the four working conditions is closely related to the acoustic emission signal, and the value of acoustic emission characteristic parameters increases with the increase of radial wear degree of the bar. This is because the radial wear degree characterizes the wear depth of the contact zone between the fixture and the bar. The greater the radial wear degree is, the more severe the extrusion effect of the fixture on the bar surface and the

wear characteristics are. So the acoustic emission characteristic parameters increase accordingly.

The amplitude in Fig. 15(a) reflects the intensity of extrusion and collision of the surface asperity when the friction pair is worn under the condition of acoustic emission monitoring. The energy in Fig. 15(b) reflects the energy released by the random extrusion collision of the surface asperity when the friction pair is worn. Fig. 15(c) and (d) show the wear characteristics of the friction pair. It can be seen from Fig. 15 that when the contact condition remains unchanged, the amplitude, energy, RMS and ASL of acoustic emission characteristic parameters increase slightly at first, then decrease to the minimum, and then increase continuously with the change of the surface roughness Ra of fixture, and the value of acoustic emission characteristic parameters is the minimum when Ra=0.4μm. Therefore, under different contact conditions, when the fixture surface roughness Ra=0.4μm, the wear characteristics of the friction pair is optimal.

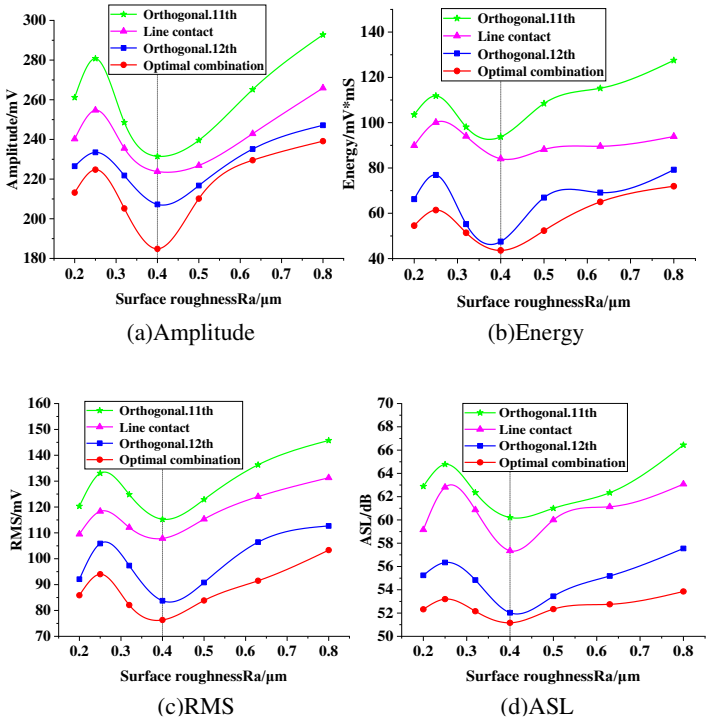

Fig. 15 Relationship between fixture roughness and AE characteristic parameters under four contact conditions

5 Conclusions

(1) The new fixture of cambered grooving structure in low-stress precision cropping is proposed and the influence of different contact parameters on the wear characteristics of friction pair is researched. The results indicate that the contact parameter that has the greatest influence on the wear quantity is the width of V-grooves b, and that the contact parameter has the greatest influence on the axial sliding distance is the number of auxiliary friction grooves, in which the auxiliary friction grooves can reduce the axial sliding distance of bars and wear at the same time. On this basis, the optimal contact parameter scheme of orthogonal test is obtained as A4B1C2D1E4, that is, h=3.0mm, b=1.4mm, r=0.3mm, α=45°, and the number of auxiliary friction grooves is 12.

(2) The radial wear degree is proposed to evaluate the wear characteristics of the bar surface under four contact conditions. The results show that the radial wear degree of the bar is the lowest at the optimal contact, which is 0.0469mm2. In the orthogonal group No. 11 contact condition, the maximum radial wear degree is 0.1034mm2. Compared with the linear contact condition, the radial wear degree of the bar is reduced by 34.50% under the optimal contact condition, and not all

cambered grooving is better than the linear contact condition.

(3) SEM consequence shows that under four contact conditions, due to the extrusion of the fixture and the bending action of the hammer head, the bar has slight sliding, and the surface has different degrees of scratches, plowings, plastic deformation, adhesive block and other microscopic morphological characteristics. At the beginning, due to the action of small plowings, the abrasive particles and adhesive wear occur on the bar surface, and the smaller abrasive particles have little effect on the oxide layer on the bar surface. With the continuous action of the load, the adhesive block on the surface of the bar is gradually oxidized after being damaged, and then oxidized wear occurs. Therefore, the wear mechanism of fixture-bar friction pair is fretting wear.

(4) The AE characteristic curve results indicate that the Amplitude, Energy, RMS and ASL increase with the increase of radial wear degree of bars. Under the same contact condition, when the surface roughness Ra of the fixture is changed, the AE characteristic parameters all show a trend of first increasing, then decreasing and then increasing. When Ra=0.4μm, the AE characteristic parameters are all the smallest, and the comprehensive wear characteristics of the friction pair is the best.

Declarations

Conflict of interest: The authors declare that they have no known competing financial interests or personal relationships that could have appeared to influence the work reported in this paper.

Acknowledgement

The author wishes to express gratitude to the National Natural Science Foundation of PR China (Approval No. 51575532), which has supported this work.

References

[1] Yao F. Advanced manufacturing technology. Tsinghua University Press, Beijing (2011)

[2] Hu Y, Hua L. Forging process and mold design. China Forestry Publishing House, Peking University Press, Beijing (2006)

[3] Zhang L, Zhang D, Wang H, et al. Research on Variable Frequency-Loading Curve in Precision Cropping System with High speed and Centrifugal Action. Int J Adv Manuf Tech. 97(5), 2969-2978 (2018) doi:10.1007/s00170-018-1999-5.

[4] Zhang L, Chen X, Wang H, et al. Research on Critical Loading Force in Precision Cropping System Based on Hydraulic Compensation [J]. Int J Mech Sci. 44-50, 142-143 (2018) doi:10.1016/j.ijmecsci.2018.04.039.

[5] Zhang L, Zhang J, Jin Y, et al. Influence of eccentric incision on crack initiation and propagation of metal bars. J Cent South Univ. 51(05), 1245-1254 (2020) doi:10.11817/j.issn.1672-7207.2020.05.009.

[6] Chen X, Zhang L, Zhang D, et al. Influence rule of loading parameters on crack initiation at the tip of V-shaped notch of bars based on XFEM. Journal of Plasticity Engineering. 25(04), 254-261 (2018) doi:10.3969/j.issn.1007-2012.2018.04.037.

[7] Xiao P, Xiong X, Ren Y. Effect of Braking Speed on Friction Properties of C/C-SiC Composites. Tribology. 26(1), 12-17 (2006) doi:10.3321/j.issn:1004-0595.2006.01.003.

[8] Zhang L, Han L, Zhang D, et al. Tribological Performance Analysis of Circular Hammerhead-bar Friction Pair in Precision Blanking. China Mechanical Engineering. 31(04), 410-416, 424 (2020) doi:10.3969/j.issn.1004-132X.2020.04.006.

[9] Zhang L, Han L, Zhang D, Li Z, et al. Friction and Wear Characteristics and Mechanism Analysis of Load and Nano MoS2 Additive on Circular Hammerhead-Bar. Tribology. 39(06), 777-

785 (2019) doi:10.16078/j.tribology.2019128.
[10] Zhu X, Pan J, Zhao X, Ren R. Effect of Contact Stress on the Evolution and Properties of FCB Wheel Steel. Tribology:1-20(2021) doi:10.16078/j.tribology.2020150.
[11] Li J, Li C, Duan Z. Effect of MoS2-Ag-V2O5 on friction and wear properties of nickel-based composites. Powder Metallurgy Technology. 39(2), 141-146 (2021) doi:10.19591/j.cnki.cn11-1974/tf.2019120008.
[12] Gong T, Yao P, Xiao Y, Fan K, Tan H, et al. Wear map for a copper-based friction clutch material under oil lubrication. Wear. 328-329, 270-276 (2015) doi:10.1016/j.wear.2015.02.055.
[13] Mukhacheva T L, Belkin P N, Dyakov I G, Kusmanov S A Wear mechanism of medium carbon steel after its plasma electrolytic nitrocarburising. Wear. 462-463 (2020) doi:10.1016/j.wear.2020.203516.
[14] Medabalimi S R, M.R. Ramesh, Kadoli R. Developing partially oxidized NiCr coatings using the combined flame spray and plasma spray process for improved wear behaviour at high temperature. Wear. 478-479 (2021) doi:10.1016/J.WEAR.2021.203885.
[15] Lu J, Li Y, Wang Y, Fu Y. Effect of Pre-impregnated Organosilicon Layer on Friction and Wear Properties of Paper-based Friction Materials. Wear. 6-13, 416-417 (2018) doi:10.1016/j.wear.2018.09.009.
[16] Slawomir W, Waldemar K, Pawel P. The effect of graphite surface texturing on the friction reduction in dry contact. Tribol Int. 151 (2020) doi:10.1016/j.triboint.2020.106535.
[17] Li H, Jia Y, Zhang D, et al. Heat production characteristic of power lithium iron phosphate batteries [J]. Chinese Journal of Power Sources. 40(5), 968–970,1083 (2016) doi:10.3969/j.issn.1002-087X.2016.05.008.
[18] Wang R, Li Y. Wear of Hot Extrusion Die for Large Diameter Thick-walled Pipes. Journal of Mechanical Engineering. 55(10), 70-76 (2019) doi:10.3901/JME.2019.10.070.
[19] Xiang G, Han Y, He T, Wang J, Xiao K. A Dynamic Wear Model for Micro-Grooved Water-Lubricated Bearings Under Transient Mixed Lubrication Condition. Journal of Tribology. 142(7), (2020) doi:10.1115/1.4046175.
[20]Cláudio R, Ávila D, Giuseppe P. Uncertainty analysis on the wear coefficient of Archard model. Tribol Int. 41(6), 473-481 (2007) doi:10.1016/j.triboint.2007.10.007.
[21] Wen S. Principles of Tribology. Tsinghua University Press, Beijing (1990)
[22] Yu H, Wang H, Yin Y., Song Z, Zhou X, et al. Tribological behaviors of natural attapulgite nanofibers as an additive for mineral oil investigated by orthogonal test method. Tribol Int. 153 (2021) doi:10.1016/j.triboint.2020.106562.
[23] Jia X, Guo F, Huang L, Richard F. Salant, Wang Y. Parameter analysis of the radial lip seal by orthogonal array method. Tribol Int. 64, 96-102 (2013) doi:10.1016/j.triboint.2013.03.005.
[24] Walker J C, Cinti S, Kamps T J, Mitchell-Smith J, Clare A T. Influence of contact zone on the sliding friction and wear behaviour of an electrochemical jet textured Al-Si alloy. Wear. 426-427,1336-1344 (2019) doi:10.1016/j.wear.2019.01.008.
[25] Egidijus K, Rostislav C, Miloslav L, Jiři K. Sensitivity analysis of the influence of particle dynamic friction, rolling resistance and volume/shear work ratio on wear loss and friction force using DEM model of dry sand rubber wheel test. Tribol Int. 156 (2021) doi:10.1016/J.TRIBOINT.2021.106853.
[26] Yang N, Tao J, Fu S, Yang B, Wang H, Guo W, Xu J, Zhang L. Research on the deflection of metal bar with V-shaped notch in low-stress cropping process. Theor Appl Fract Mec. 114(103017),

1-12 (2021) https://doi.org/10.1016/j.tafmec.2021.103017.
[27] Xu F, Fu R, Fan J, Wang Y, Li W. Mechanics of Materials. Nanjing Southeast University Press, Nanjing (2017)
[28] Pan S, Zhao C, Wei P, Ren F. Sliding wear of CoCrNi medium-entropy alloy at elevated temperatures: Wear mechanism transition and subsurface microstructure evolution. Wear. 440-441 (2019) doi:10.1016/j.wear.2019.203108.
[29] Duan Y, Qu S, Jia S, Li X. Evolution of wear damage in gross sliding fretting of a nitrided high-carbon high-chromium steel. Wear. 464-465 (2021) doi:10.1016/j.wear.2020.203548.
[30] Belkhir N, Bouzid D, Herold V. Correlation between the surface quality and the abrasive grains wear in optical glass lapping. Tribol Int. 40(3), 498-502 (2007) doi:10.1016/j.triboint.2006.05.001.
[31] Wang D, Yang J, Wei P, Pu W. A mixed EHL model of grease lubrication considering surface roughness and the study of friction behavior. Tribol Int. 154 (2021) doi:10.1016/J.TRIBOINT.2020.106710.
[32] K V, Mathew J. Wear behavior of TiAlN coated WC tool during micro end milling of Ti-6Al-4V and analysis of surface roughness. Wear. 424-425, 165-182 (2019) doi:10.1016/j.wear.2019.02.018.
[33] Fan Y, Gu F, Ball A. Modelling acoustic emissions generated by sliding friction. Wear. 268(5), 811-815 (2009) doi:10.1016/j.wear.2009.12.010.
[34] Puliyakote S, Singanamalli A V, Balasubramaniam K. Use of acoustic emission in lubrication monitoring in internal combustion engines. Insight. 56(1), 22-24 (2014) doi:10.1784/insi.2014.56.1.22.